ELSEVIER

Journal of Nuclear Materials 317 (2003) 217–225

journal of nuclear materials

www.elsevier.com/locate/jnucmat

Mechanical behaviour of macro-dispersed inert matrix fuels

E.A.C. Neeft [a], K. Bakker [a], R.L. Belvroy [a], W.J. Tams [a], R.P.C. Schram [a,*], R. Conrad [b], A. van Veen [c]

[a] *NRG, P.O. Box 25, 1755 ZG Petten, The Netherlands*
[b] *Joint Research Centre IE, P.O. Box 2, 1755 ZG Petten, The Netherlands*
[c] *Interfaculty Reactor Institute, Mekelweg 15, 2629 JB Delft, The Netherlands*

Received 7 March 2002; accepted 14 February 2003

Abstract

Macro-dispersed inert matrix fuels were irradiated in the high flux reactor in Petten. These fuels consisted of UO_2 inclusions embedded in the inert matrices MgO, $MgAl_2O_4$, $Y_3Al_5O_{12}$, CeO_{2-x} and Y_2O_3. The uranium burn-up reached 17.1–19.8% FIMA after an irradiation period of 198.9 days. The sample temperature was about 700–1000 K. Room temperature indentation measurements were performed in the inert matrices before and after irradiation to determine the Vickers hardness and the fracture toughness. The volume swelling of the UO_2 inclusions has been determined. Pellets of UO_2 inclusions embedded in MgO, $MgAl_2O_4$ and $Y_3Al_5O_{12}$ show cracks in the matrix between these inclusions after neutron irradiation. A model is used to describe the fracture behaviour of these inert matrix fuels.

1. Introduction

Transmutation of long-lived actinides (e.g. plutonium and americium) in uranium-free matrices is a promising option to reduce the radiotoxicity of long-lived nuclear waste. Within the EFTTRA-framework (Experimental Feasibility of Targets for Transmutation, A European project in which CEA, NRG, EdF, FzK, JRC-ITU and JRC-IE co-operate), the application of inert matrix fuel for actinide transmutation is studied. In the EFTTRA-T3 experiment, fuels containing UO_2 inclusions embedded in a matrix were irradiated in the high flux reactor. In the present paper, the mechanical aspects of such fuels are discussed. A general description of the EFTTRA-T3 experiment including all results of the PIE is given by Neeft et al. [1].

In the present irradiation experiment (EFTTRA-T3) uranium simulates some of the effects of the actinides to be transmutated (e.g. plutonium or americium). An advantage is that uranium can be handled more easily than plutonium or americium containing material. The aim of this experiment is to study the effect of fission products on the fuel behaviour. Inert matrices with and without uranium were irradiated to discriminate the effect of fission products from that of neutrons. It is not the aim to be fully representative for the conditions in any future large-scale industrial transmutation scenarios. Due to the rather general aim of the present experiment, the results are relevant to both LWR and fast reactor applications.

The present paper focuses on the mechanical behaviour of the macro-dispersed composite fuels. The fuels considered are composite materials, which consist of a ceramic fissile phase embedded in an inert ceramic matrix phase. The mechanical behaviour of the composite fuels is more complicated than that of homogeneous fuels such as UO_2. A good understanding of the mechanical properties of the fuels is important since swelling and fracture of the pellets have a strong influence on amongst others the temperature of the fuel, fission-gas release and the

* Corresponding author. Tel.: +31-224 564 362; fax: +31-224 568 608.
E-mail address: schram@nrg-nl.com (R.P.C. Schram).

0022-3115/03/$ - see front matter
doi:10.1016/S0022-3115(03)00096-5

mechanical interaction between the fuel and the cladding.

2. Sample preparation and characterisation

2.1. Characterisation of starting materials

UO_2 microspheres were prepared by the sol–gel technique, and the particle diameter after sintering is in the order of 100–300 μm [1]. A minor fraction of very small UO_2 particles (<10 μm) is observed on the surface of the UO_2 particles. The UO_2 microspheres were separated into four size-fractions by sieving in order to measure the size distribution. The mass of each size-fraction was measured. Optical microscopy images were made of these microspheres before and after sintering in a molybdenum cup at the same conditions as for pellets with UO_2 (5 h in H_2/Ar at 1873 K). Table 1 shows the characteristics of the UO_2 microspheres as determined by image analysis. More than 80 mass% of particles are larger than 53 μm. The powders of all matrices (CeO_2, Y_2O_3, MgO, $MgAl_2O_4$ and $Y_3Al_5O_{12}$) were obtained commercially.

2.2. Sample preparation

UO_2 microspheres were mixed with powders of CeO_2, MgO, $MgAl_2O_4$, $Y_3Al_5O_{12}$ and Y_2O_3 in a mortar. All fuels contained about 2.5 vol.% UO_2 with a ^{235}U enrichment of 20%. The powders were uniaxially pressed into green pellets and these pellets were sintered for 5 h in a reducing atmosphere of H_2/Ar (5%/95%) at 1873 K. The average diameters of the sintered pellets ranged from 5.11 to 5.39 mm. An overview of the properties of samples is given in Table 2. Inert matrix pellets without UO_2 were also fabricated at similar conditions except that the sintering atmosphere was air. These pellets were used to determine the grain size of the matrix phase, as shown in Table 2. More details on preparation and characterisation are given in [1–3].

2.3. Sample characterisation

2.3.1. Ceramography

Ceramography before irradiation shows that the pellets do not contain cracks (e.g. Fig. 1). The UO_2 inclusions have a circular shape in the radial cuts and an elliptical shape in the axial cuts. This ellipsoidal shape is due to the uniaxial pressing of the pellets. The porosity of the UO_2 inclusions in the $MgAl_2O_4$ and Y_2O_3 matrices could not be measured before neutron irradiation due to outbreak during polishing. Two UO_2 inclusions embedded in $Y_3Al_5O_{12}$ and MgO showed a porosity of 1% and 10%, respectively. In the $Y_3Al_5O_{12}$ and $MgAl_2O_4$ matrices, gaps surrounding the UO_2 inclusions were observed, which is due to different sintering behaviour of the UO_2 inclusions and the matrix.

2.3.2. X-ray diffraction

X-ray diffraction was performed prior to irradiation. An assessment [1] of these results was made for the EFTTRA-T3 irradiation using phase diagrams, which leads to the following conclusions:

Table 1
Characteristics of the UO_2 microspheres

	Sieve mesh size ∅ (μm)			
	∅ > 150	150 > ∅ > 53	53 > ∅ > 25	∅ < 25
Mass fraction	0.4882	0.3688	0.0896	0.0535
Average particle diameter (μm) (calculated using average volume)				
Before sintering	288	168	63.30	9.63
After sintering	193	112	42.17	9.54
Volume swelling (%) after sintering	−69.8	−70.1	−70.4	−2.9

Table 2
Properties of the samples and neutron fluence

Pin	Compound	Density (% TD)	Grain size, matrix phase (μm)	Neutron fluence (10^{25} m^{-2})	
				Thermal	Fast ($E > 0.1$ MeV)
1	$CeO_{2-x} + UO_2$	86.6 ± 1.9	10–30	2.83	5.89
18	$Y_2O_3 + UO_2$	94.6 ± 1.0	10–20	2.86	6.17
5	$MgO + UO_2$	89.2 ± 2.5	2–5	2.89	6.23
11	$MgAl_2O_4 + UO_2$	95.3 ± 0.8	2–5	3.44	7.18
15	$Y_3Al_5O_{12} + UO_2$	90.4 ± 0.7	2–5	3.41	6.93

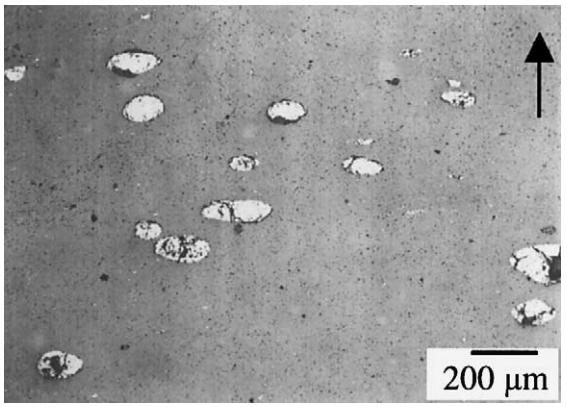

Fig. 1. Axial cut of an unirradiated $MgAl_2O_4 + UO_2$ pellet. The arrow marks the axial direction of the pellet.

1. No chemical interaction occurred between UO_2 and the matrices MgO, $MgAl_2O_4$ and $Y_3Al_5O_{12}$ after sintering of the pellets.
2. Some chemical interaction occurred between UO_2 and the Y_2O_3 and CeO_{2-x} matrices forming the solid solutions $(U,Y)O_{2-x}$ and $(Ce,U)O_{2-x}$ which are present beside the initial phases UO_2, Y_2O_3 and CeO_{2-x}.
3. Due to the sintering under hydrogen of the $CeO_2 + UO_2$ sample, the cerium-oxide phase is probably somewhat sub-stoichiometric CeO_{2-x} $(0 < x < 0.17)$. The exact sub-stoichiometry has not been determined.

3. Neutron irradiation

The pellets were loaded in capsules with an inner diameter of 5.65 mm and an outer diameter of 6.55 mm. The pellet stack had a length of about 70 mm. The experimental set-up for the neutron irradiation in EFT-TRA-T3 is described in Neeft et al. [1]. The neutron fluence was measured using neutron monitor sets and is shown in Table 2. The burn-up of the samples after 198.9 effective full power days was calculated using FISPACT [4] to be 17.1–19.8% fissions per initial metal (uranium) atom (FIMA). The temperature of the UO_2-containing targets during irradiation was estimated to be 700–1000 K. The linear power was at start 45–63 W cm^{-1} and decreased to 16–23 W cm^{-1} at the end of the irradiation. The calculated temperature of pellets without UO_2 is about 640–690 K.

4. Experimental results

4.1. Ceramography after irradiation

The irradiated $Y_2O_3 + UO_2$ and the $CeO_{2-x} + UO_2$ pellets have only a few cracks (Fig. 2). These cracks can be attributed to thermal stress in the pellets, similar to

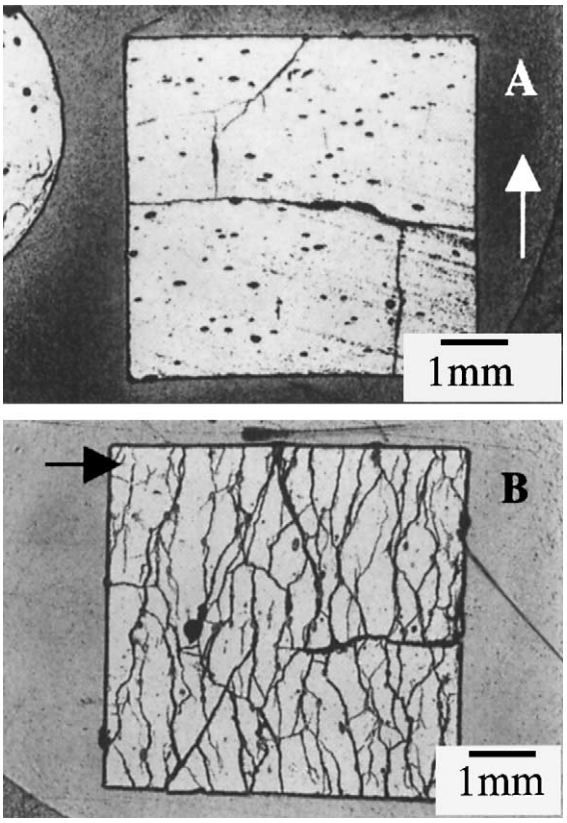

Fig. 2. Irradiated pellets of (A) $Y_2O_3 + UO_2$ and (B) $MgAl_2O_4 + UO_2$ (arrow: axial direction of pellet).

irradiated UO_2 pellets. The pellets of UO_2 in $MgAl_2O_4$, MgO and $Y_3Al_5O_{12}$ show a high density of cracks (Fig. 2), which run between the UO_2 inclusions.

Fig. 3 shows the UO_2 inclusions embedded in the Y_2O_3 and $MgAl_2O_4$ matrices. The UO_2 inclusions kept their ellipsoidal shape during irradiation. The cracks between the UO_2 inclusions in the matrices MgO, $MgAl_2O_4$ and $Y_3Al_5O_{12}$ do not penetrate through the UO_2 inclusions. The white circles in Fig. 3 show for $MgAl_2O_4$ and $Y_3Al_5O_{12}$ that the cracks in the matrix start some distance away from the interface between the matrix and the UO_2 inclusion. This might be induced by a locally enhanced creep of the matrix, due to the implantation of fission products. This local presence of fission products in the matrix is due to the 10 μm recoil range of fission products from the UO_2 inclusions, which is in agreement with EPMA results [1,5].

A high porosity is observed in the irradiated UO_2 particles, in which a considerable fraction of the porosity is caused by a few large pores (Fig. 3). This high porosity is in good agreement with that observed in the high burn-up rim region of UO_2 pellets. After a burn-up of 170 MWd/kg U in the rim region, 50% porosity were observed in UO_2 [6]. The temperature conditions of the

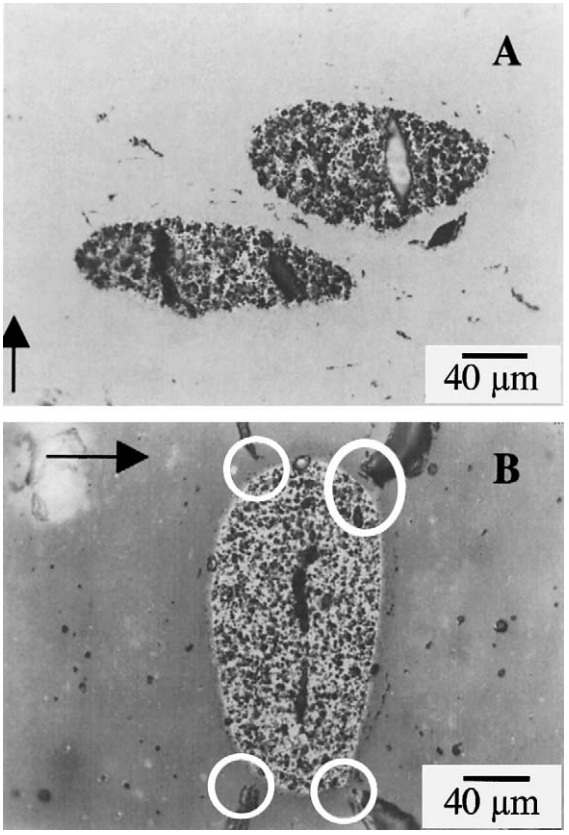

Fig. 3. UO_2 inclusions after irradiation in the matrices (A) Y_2O_3 and (B) $MgAl_2O_4$. The white circles indicate intact matrix material (arrow: axial direction of pellet).

irradiated UO_2 in the present study are similar to those in the rim region.

4.2. α-Autoradiography after irradiation

After neutron irradiation, α-autoradiographs of these samples were made. Fig. 4 shows the α-autoradiographs of $Y_2O_3 + UO_2$ and $MgAl_2O_4 + UO_2$; those of UO_2 in $MgAl_2O_4$, MgO and $Y_3Al_5O_{12}$ show only areas of α-emission at the location of UO_2 inclusions. The α-autoradiographs of UO_2 embedded in CeO_{2-x} and Y_2O_3 show besides α-emission from UO_2 inclusions also grey areas in the matrices. These areas are caused by a low concentration of uranium present in the matrix, which can be understood by the formation of the $(U,Y)O_{2-x}$ and $(Ce,U)O_{2-x}$ solid solutions observed by X-ray diffraction (Section 2.3.2).

4.3. Porosity and swelling of the UO_2 inclusions

The swelling of the UO_2 inclusions after neutron irradiation is determined using two methods of which the

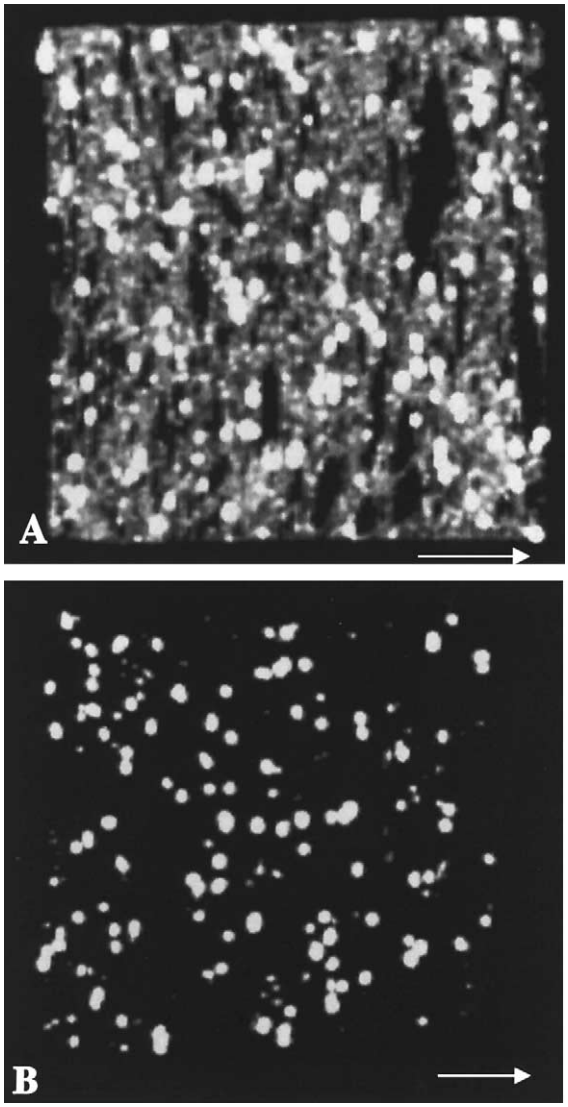

Fig. 4. The α-autoradiographs of a (A) $Y_2O_3 + UO_2$ and (B) $MgAl_2O_4 + UO_2$ pellet shown in Fig. 2(A) and (B), respectively. (arrow: axial direction of pellet), the width of the figures is about 5 mm.

results are shown in Table 3. The two methods to determine the swelling are described hereafter:

Method A: The swelling of the UO_2 inclusions can be determined by measuring the area of the inclusions before and after neutron irradiation in the ceramographic cuts using image analysis. Comparison of these data yields the volume swelling.
Method B: The swelling of the UO_2 inclusions is the sum of the swelling induced by solid fission products and that induced by porosity (Appendix A). The swelling of UO_2 induced by solid fission

Table 3
Porosity and swelling data

Composite	Porosity after irradiation (%)	Volume swelling (%)	
		Method A	Method B
$CeO_{2-x} + UO_2$	32 ± 8	–	50 ± 21
$Y_2O_3 + UO_2$	27 ± 10	–	40 ± 22
$MgO + UO_2$	–	47 ± 17	–
$MgAl_2O_4 + UO_2$	39 ± 6	74 ± 22	68 ± 20
$Y_3Al_5O_{12} + UO_2$	42 ± 4	–	77 ± 17

products is about 0.5 vol.% per 10 GWd/t [7]. Table 3 shows the porosity of the UO_2 inclusions in the matrices after irradiation as determined by image analysis. The porosity of the UO_2 inclusions before irradiation is $5.5 \pm 6.4\%$, as obtained from image analysis on two of the samples (Section 2.3.1). A UO_2 porosity of 5.5% is also in agreement with the 5% porosity, which is generally observed in UO_2 pellets sintered under similar conditions.

Due to the insufficient quality of the microscopy images (due to outbreak) the two techniques could not be applied for all samples. The following conclusions can be drawn from Table 3.

- The porosity in the UO_2 phase ranges between 30 and 40 vol.% after neutron irradiation.
- The swelling of the UO_2 particles ranges between about 50 and 80 vol.%.
- The swelling results obtained using the two above-mentioned methods show reasonable agreement.

4.4. Indentation measurements

4.4.1. Method

Room temperature indentation measurements were performed on the matrices in order to determine the Vickers hardness and the fracture toughness. The measurements were performed at least 30 μm from the UO_2 particles in order to avoid an influence of the fission products. Indentation loads of 100 and 200 g were applied. The load rate was about 1–2 $g\,s^{-1}$ and the load was applied for 10 s. The Vickers hardness (H_V, in $kg\,mm^{-2}$) has been determined using [8]:

$$H_V = 1.8544 \frac{M}{\{2a\}^2}, \quad (1)$$

where M is the indentation load in kg and $\{2a\}$ is the imprint diagonal in mm. The fracture toughness (K_{IC}) in $MPa\,m^{1/2}$ is calculated using [9]:

$$K_{IC} = \left\{ \frac{0.035 H_V \sqrt{a}}{\Phi} \right\} \left\{ \frac{E\Phi}{H_V} \right\}^{0.4} \left\{ \frac{l}{a} \right\}^{-0.5}, \quad (2)$$

where H_V is in MPa, l is the crack length, l and a both in meters, E is the Young modulus in MPa and Φ is the constraint factor with a value of 2.7 [10]. This equation is valid for $0.25 < l/a < 2.5$. The crack length l is measured parallel along the diagonal of the indent. For each matrix 5–10 indents were made.

In order to calculate the fracture toughness (Eq. (2)), data on the Young modulus are required. Since the Young modulus has not been determined for the present samples, literature data of unirradiated 100% dense materials have been corrected for the porosity in the present samples. This correction has been done using an empirical relation determined for Y_2O_3 [15] and MgO [12]. For $MgAl_2O_4$, CeO_{2-x} and $Y_3Al_5O_{12}$ the relation of Morrell [8] is used. The input data and the applied Young's modulus are shown in Table 4. The literature data for the Young modulus of CeO_{2-x} has been derived from the shear modulus [13]. The Poisson ratio of CeO_{2-x} (0.3) is an assumed value. Since neutron irradiation has only a small influence on the Young modulus of $MgAl_2O_4$ [14] and MgO [17] and no literature data are available for the other matrices, the impact of irradiation on the Young modulus is neglected.

4.4.2. Results of the indentation measurements

The results of the indentation measurements in the inert matrices are shown in Tables 5 and 6. Considering the distribution in size of the sintered UO_2 microspheres and a fission product penetration depth of 10 μm, it was calculated that less than 5 vol.% of the matrix is implanted with fission products. The indentations performed in the MgO, $MgAl_2O_4$ and $Y_3Al_5O_{12}$ matrices are therefore nearly only in matrix free of fission products. The indentations in CeO_{2-x} and Y_2O_3 are possibly polluted with fission products. Table 5 shows that the change in hardness of $MgAl_2O_4$ is +3%, of CeO_{2-x} is +66%, of Y_2O_3 is +16% and of $Y_3Al_5O_{12}$ is at least −30%. These data have not been corrected for a possible change in the porosity of the matrices during irradiation. A minor increase in the porosity can cause a relatively large decrease of the hardness [18]. The geometrical density of most of the UO_2 containing pellets changed during irradiation [1], which is shown in Table 5. The change in the geometrical density can be used as an

Table 4
Literature data on the Young modulus and Poisson's ratio and the Young modulus corrected for porosity

Matrix	Literature data			Applied E (GPa)
	E (GPa)	v	Reference	
CeO_{2-x}	162.4	0.3	[13]	162
MgO	317.7	0.138	[12]	197
$MgAl_2O_4$	274.0	0.269	[14]	251
$Y_3Al_5O_{12}$	278.6	0.251	[11,16]	243
Y_2O_3	180.1	0.299	[15]	159

Table 5
Results of the Vickers hardness measurements and literature data

Matrix	H_V (kg mm^{-2})			Geometrical density increase (%)
	Measured		Literature unirradiated	
	Unirradiated	Irradiated		
CeO_{2-x}	$532 \pm 155^{\#}$	$883 \pm 171^{\#}$	$387 \pm 82^{*}$ [20]	-4.9 ± 1.5
MgO		$1068 \pm 102^{\#}$ $998 \pm 37^{*}$	$760^{\#}$ [13]	0.9 ± 1.0
$MgAl_2O_4$	$1615 \pm 113^{*}$	$1663 \pm 175^{*}$	$1500^{\#}$ [8]	
$Y_3Al_5O_{12}$	$1446 \pm 67^{*}$	$1014 \pm 60^{*}$	$1835 \pm 51^{*}$ [21]	10.5 ± 1.1
Y_2O_3	$842 \pm 26^{*}$	$1066 \pm 94^{\#}$ $975 \pm 67^{*}$	739 [13] 612 [21]	-1.4 ± 0.4

Indentation mass is: $^{\#}$ 100 g, * 200 g.
Geometrical density increase represents the increase in the density of the currently studied pellets during irradiation.

Table 6
Results of the fracture toughness measurements and literature data

Matrix	K_{IC} (MPa m$^{1/2}$)		
	Measured		Literature unirradiated
	Unirradiated	Irradiated	
CeO_{2-x}	$1.2 \pm 0.2^{\#}$	$1.5 \pm 0.4^{\#}$	
MgO		$1.8 \pm 0.3^{\#}$ $2.0 \pm 0.5^{*}$	1.6–1.8 [22]
$MgAl_2O_4$	$2.5 \pm 0.4^{*}$	$2.0 \pm 0.2^{*}$	3.0 [22] 1.94 ± 0.10 [23]
$Y_3Al_5O_{12}$	$2.5 \pm 0.4^{*}$	$1.9 \pm 0.5^{*}$	1.7 ± 0.1 [21]
Y_2O_3	$1.7 \pm 0.2^{*}$	$2.1 \pm 0.4^{\#}$ $2.1 \pm 0.3^{*}$	

Indentation mass is: $^{\#}$ 100 g, * 200 g.

indication of the change in the porosity. The change in the geometrical density of $MgAl_2O_4 + UO_2$ is due to extensive fracturing of the matrix and therefore no information on the change in porosity can be obtained from these data. Comparison of the change in hardness and in geometrical density during irradiation shows a clear correlation between both data sets. Since insufficient data are available on specific material properties, such as the critical load for indentation, no correction of the hardness data for the porosity has been made.

Table 6 shows that the fracture toughness of CeO_{2-x} and Y_2O_3 increases and that of $MgAl_2O_4$ and $Y_3Al_5O_{12}$ decreases during irradiation. The measured fracture toughness is influenced by the porosity, the microstructure and the Young modulus. Porosity generally decreases the fracture toughness, but similar to the case of the hardness, the impact of a change in porosity on the fracture toughness has not been corrected for.

Indentation measurements were also done on the irradiated UO_2 inclusions. Large variations were observed for the Vickers hardness (150–980 kg mm^{-2}). The fracture toughness could not be determined since the high porosity made it impossible to determine the crack lengths. Hardness measurements on high burn-up UO_2 pellets show a decrease of the hardness and an increase of the fracture toughness with increasing burn-up [18]. A decrease in hardness has the positive consequence that the mechanical interaction between the pellets and the cladding decreases. This phenomenon has been observed for instance in a comparison of the behaviour of UO_2 and MOX fuel. The lower hardness of MOX fuel causes the power at which a MOX fuel rod fails to be higher than that of a UO_2 rod [19]. An increase in the fracture toughness has the positive consequence that the risk of extensive pellet fragmentation during normal operation or accident conditions decreases. The differences in hardness and fracture toughness of the irradiated materials are relatively small for the presently studied matrices and therefore no conclusion can be drawn from these data on the most suitable inert matrix.

Literature data on the Vickers hardness and fracture toughness of unirradiated polycrystalline materials are included in Tables 5 and 6. The literature data are in good agreement with the presently measured data on the unirradiated matrices, considering the variations in microstructure, porosity and measurement technique that exist between the various measurements.

$MgAl_2O_4$ is the only matrix for which literature data on the impact of irradiation on the hardness of polycrystalline material could be found. At an irradiation temperature of 823 K after a fast neutron fluence of 2.3×10^{24} m^{-2}, the change in hardness was 1.8% [24]. The Knoop hardness increased by 5%, 10% and 12% at 658 K after a fast neutron fluence of 2.2×10^{26}, 2.4×10^{26} and 24.9×10^{26} m^{-2}, respectively [25]. $MgAl_2O_4$ was

exposed in the present study to a fast fluence ($E > 0.1$ MeV) of 7.18×10^{25} m^{-2} and the slight increase in hardness $(3 \pm 5)\%$ is in good agreement with the other studies. No data could be found on the impact of irradiation on the fracture toughness of the polycrystalline materials.

4.4.3. Discussion on fracture behaviour

During irradiation, cracks were formed between the UO_2 inclusions in the $Y_3Al_5O_{12}$, $MgAl_2O_4$ and MgO matrices. Lutz and Claussen [26] studied the fracture behaviour of ceramic composites containing particles. In this theory the thermal expansion of particles and matrix is considered in relation to the cracking behaviour. This model (Appendix B) is considered to be applicable for a matrix containing swelling particles, in which a slight modification of the condition for crack formation is included. In the present paper this theory is applied for the first time to predict the crack behaviour in composite fuels. The formation of cracks is favoured by larger inclusions, higher Young's moduli and lower Poisson's ratios for both matrix and inclusions and smaller values of fracture toughness of the matrix. A difference in thermal expansion between the UO_2 particles and the matrix might also cause fracture. However, for the present case this thermal expansion cannot result into fracture of the matrix.

The swelling of a UO_2 inclusion (diameter of 200 μm) at which fracture from inclusion to inclusion is expected to occur according to the model in Appendix B is 1.8–2.6 vol.%. The swelling of the UO_2 inclusions are 50–80 vol.% (Table 3) and therefore fracture is expected in all UO_2 containing matrices. However, for $CeO_{2-x} + UO_2$ and $Y_2O_3 + UO_2$ no such fracture is observed (Fig. 3(A)). The absence of fracture of the matrix can only be due to creep of the matrix. In for instance $MgAl_2O_4 + UO_2$ fracture of the matrix is observed (Fig. 3(B)). The white circles in Fig. 3(B) mark a region in $MgAl_2O_4$ where the implantation of fission products apparently strongly enhanced the creep rate, since locally the matrix was not fractured. α-Autoradiographs of $CeO_{2-x} + UO_2$ and $Y_2O_3 + UO_2$ showed some α-emission from the matrix, which indicates the presence of a low concentration of fission products in the CeO_{2-x} and Y_2O_3 matrix. No α-emission was observed in the other matrices and therefore no fission product implantation is expected. The implantation of fission products in the CeO_{2-x} and Y_2O_3 matrix may have enhanced the creep rate and thereby might have prevented crack formation. As the UO_2 inclusions swelled about 50–80 vol.%, there can be no other explanation than that the volume of these matrices decreased by creep to obtain space for the swelling UO_2 inclusions. In the model in Appendix B the possibility of creep of the matrix (e.g. MgO [27]) is not taken into account.

Cracks between the UO_2 inclusions are mainly aligned in the radial direction (e.g. Fig. 2, $MgAl_2O_4 + UO_2$). This orientation of the cracks can probably be attributed to the orientation of the ellipsoidal UO_2 inclusions. Dimensional measurements showed that this crack orientation increased the height of the pellets more than the diameter [1,3]. Swelling only in the axial direction has the advantage that cladding deformation is prevented.

5. Conclusions

The EFTTRA-T3 irradiation experiment has been completed successfully giving interesting information on the mechanical behaviour of inert matrix fuels. Cracks from UO_2 inclusion to UO_2 inclusion are observed after neutron irradiation in the $Y_3Al_5O_{12}$, MgO and $MgAl_2O_4$ matrices. The formation of these cracks can be explained by swelling of the UO_2 inclusions. The Y_2O_3 and CeO_{2-x} matrices do not show cracks from UO_2 inclusion to UO_2 inclusion. According to a simple mechanical model cracks are expected in all matrices considering the swelling of the UO_2 phase. The origin of this behaviour found for CeO_{2-x} and Y_2O_3 is not yet fully clear, but is possibly related to fission-induced creep. The absence of the crack behaviour is a good property from the point of view of the fuel behaviour and therefore it can be concluded that the mechanism for the absence of fracture in these two matrices should be studied in more detail.

Irradiation increases the fracture toughness of CeO_{2-x} and Y_2O_3 and decreases the fracture toughness of $MgAl_2O_4$ and $Y_3Al_5O_{12}$. The hardness of CeO_{2-x} and Y_2O_3 increases, that of $MgAl_2O_4$ remains constant and that of $Y_3Al_5O_{12}$ decreases upon irradiation. However, it should be noted for all inert matrices studied that the hardness values and the fracture toughness values, both before and after irradiation, are in the range 500–1700 $kg\,mm^{-2}$ and 1–3 $MPa\,m^{1/2}$, respectively. It can be concluded that no extremely large variation exists in the properties of these matrices and that, based on these hardness and fracture toughness measurements, no selection can be made as to one inert matrix being more suitable as another inert matrix.

Acknowledgements

The authors would like to thank H. Hein, R.J.M. Konings and J.G. Boshoven for the fabrication of the targets. M.R. Roos is acknowledged for the measurements of porosity of the UO_2 inclusions, P. van Vlaanderen for the X-ray analysis and J.R.W. Woittiez, B. Beemsterboer and O. Zwaagstra for the INAA analysis, A. Paardekooper for the neutron metrology and C. Sciolla for the nuclear calculations.

Appendix A. Swelling of the UO_2 inclusions

The swelling of the UO_2 inclusions is calculated by combining the data on swelling induced by solid fission products and by an increase in porosity (method B). The volume of the solid material in an inclusion before irradiation ($V_{\text{solid,before}}$) can be described by:

$$V_{\text{solid,before}} = V_{\text{total,before}}\{1 - P_{\text{before}}\}, \tag{A.1}$$

where P is the porosity in the inclusions before irradiation and $V_{\text{total,before}}$ is the total volume of the inclusion before irradiation. A similar relation holds after irradiation. The solid volume after neutron irradiation ($V_{\text{solid,after}}$) is related to the solid volume before neutron irradiation by:

$$V_{\text{solid,after}} = V_{\text{solid,before}}\left\{1 + \frac{\Delta V}{V_{\text{solid}}}\right\}, \tag{A.2}$$

where $\Delta V/V_{\text{solid}}$ is the solid fission product swelling, which is about 0.5% per 10 GWd/t [7]. This value is multiplied by the burn-up in EFTTRA-T3 and a minor correction is applied for the fraction of solid fission products that are implanted directly in the matrix after fission. Combining the equations results in

$$\frac{\Delta V^B}{V} = \left\{\left(1 + \frac{\Delta V}{V_{\text{solid}}}\right)\left(\frac{1 - P_{\text{before}}}{1 - P_{\text{after}}}\right)\right\} - 1, \tag{A.3}$$

where P_{after} is the porosity of the UO_2 inclusions after irradiation. The volume change by porosity swelling is usually calculated by subtraction of porosity before neutron irradiation from the porosity after neutron irradiation. For small values of porosity, this mathematically wrong method gives negligible deviation from the volume swelling compared to the previously described equation. In the present study, the porosity is very large, therefore this method was used.

Appendix B. Swelling of spherical particles in a matrix

The formation of cracks in a matrix containing single-sized spherical particles (radius R_p, volume fraction V_p) of which the volume tends to strain with respect to the matrix is described in Lutz and Claussen [26]. This volume strain can be a combination of two effects:

- Increase of the volume due to swelling as observed in the present study.
- A larger thermal expansion of the particle than that of the matrix upon heating.

The volumetric strain of the particle (ε_v) is defined by:

$$\varepsilon_v = \frac{\Delta V}{V} + 3\,\Delta T(\alpha_p - \alpha_m), \tag{B.1}$$

where $(\Delta V/V)$ is the increase in volume of the particle by swelling, α_p and α_m are the linear thermal expansion coefficients of particle and matrix, respectively. ΔT is the temperature difference over which the complete ceramic composite is heated (or cooled), assuming that the temperature of the particles and the matrix is identical. For the present study ΔT is maximum 700 K, being the maximum temperature difference of the centre of the fuel during irradiation and before or after irradiation. For the conditions of the EFTTRA-T3 experiment the temperature difference and the difference in thermal expansion is not sufficiently large to induce fracture. The swelling of the particles causes stress at the interface between the matrix and the particle. When the stress is sufficiently large annular cracks are formed in the matrix surrounding the particles. This means that the particles themselves remain intact. The condition for inter-particle fracture is:

$$\left[\frac{\beta R_p(\beta+2)}{\pi(\beta+1)}\right]^{1/2}\left[\left(\frac{1}{(\beta+1)^2} + \frac{6\sqrt{2}}{\pi}V_p\right)c_4\right] > K_{IC}. \tag{B.2}$$

Eq. (B.2) contains the following variables: $\beta = (R_m/R_p) - 1$, where R_m (the effective half-distance between the particles) is defined as:

$$\sqrt[3]{\frac{\pi/3\sqrt{2}}{V_p}}R_p^3,$$

K_{IC} is the fracture toughness of the matrix material.

$$c_4 = \frac{c_1}{c_2 + c_3(R_p/R_m)^3},$$

where $c_1 = 2/3E_pE_m\varepsilon_v$, $c_2 = 2E_m(1 - 2\nu_p) + E_p(1 + \nu_m)$ and $c_3 = 2[E_p(1 - 2\nu_m) - E_m(1 - 2\nu_p)]$ in which E_p and E_m are the Young moduli of the particle and the matrix, ν_p and ν_m are the Poisson ratios of the particle and the matrix.

References

[1] E.A.C. Neeft, K. Bakker, R.P.C. Schram, R. Conrad, R.J.M. Konings, J. Nucl. Mater., in press.
[2] R.J.M. Konings, K. Bakker, J.G. Boshoven, H. Hein, M.E. Huntelaar, R.R. van der Laan, J. Nucl. Mater. 274 (1999) 84.
[3] E.A.C. Neeft, K. Bakker, H.A. Buurveld, J. Minkema, A. Paardekooper, R.P.C. Schram, C. Sciolla, O. Zwaagstra, B. Beemsterboer, J.R.W. Woittiez, P. van Vlaanderen, W.J. Tams, H. Hein, R. Conrad, A. van Veen, Prog. Nucl. Energy 38 (2001) 427.
[4] R.A. Forrest, J.Ch. Sublet, UKAEA-report: UKAEA FUS 287, July 1995.
[5] K. Bakker, R. Belvroy, F.A. van den Berg, S. Casalta, R. Conrad, E.A.C. Neeft, R.P.C. Schram, W.J. Tams, Prog. Nucl. Energy 38 (2001) 313.

[6] W. Wiesenack, T. Tverberg, in: Proceedings of the 2000 International Topical Meeting on LWR Fuel Performance, Park City, Utah, 10–13 April, American Nuclear Society, 2000.
[7] K. Une, M. Hirai, K. Nogita, T. Hosokawa, Y. Suzawa, S. Shimizu, Y. Etoh, J. Nucl. Mater. 278 (2000) 54.
[8] R. Morrell, Handbook of Properties of Technical and Engineering Ceramics, 1st Ed., 1985, p. 128, 133.
[9] K. Niihara, R. Morena, D.P.H. Hasselman, J. Mater. Sci. Lett. 1 (1982) 13.
[10] A.G. Solomah, L. Esposito, Eur. Appl. Res. Rept.-Nucl. Sci. Technol. 7 (1990) 1441.
[11] M.M. Kuklja, R. Pandey, J. Am. Ceram. Soc. 82 (1999) 2881.
[12] J.B. Wachtman, Mechanical Properties of Ceramics, 10th Ed., 1996, p. 24, 410.
[13] G.V. Samsonov, The Oxide Handbook, PP, NY, 1982, p. 183.
[14] F.A. Garner, G.W. Hollenberg, F.D. Hobbs, J.L. Ryan, J. Nucl. Mater. 212–215 (1994) 1087.
[15] O. Yeheskel, O. Tevet, J. Am. Ceram. Soc. 82 (1999) 136.
[16] U.W. Suter, B.E. Eichinger, Polymer 43 (2002) 575.
[17] M. Stevanovic, J. Elston, Proc. Brit. Ceram. Soc. 7 (1967) 423.
[18] Hj. Matzke, J. Spino, J. Nucl. Mater. 248 (1997) 170.
[19] W. Goll, H. Fuchs, R. Manzel, F.U. Schlemmer, Nucl. Technol. 102 (1993) 29.
[20] S. Maschio, O. Sbaizero, S. Meriani, Eur. Appl. Res. Rept.-Nucl. Sci. Technol. 7 (1990) 1495.
[21] G. de With, J.E.D. Parren, Solid State Ionics 16 (1985) 87.
[22] R.G. Munro, S.W. Freiman, T.L. Baker, National Institute for Standards and Technology, report NISTIR 6153, 1998.
[23] R.L. Stewart, R.C. Bradt, J. Am. Ceram. Soc. 63 (1980) 619.
[24] T. Yano, Y. Fukushima, H. Sawada, M. Miyazaki, T. Iseki, J. Nucl. Mater. 212–215 (1994) 1046.
[25] T. Yano, J. Am. Ceram. Soc. 82 (1999) 3355.
[26] H.E. Lutz, N. Claussen, J. Eur. Ceram. Soc. 7 (1991) 209.
[27] W.D. Kingery, H.K. Bowen, D.R. Uhlmann, Introduction to Ceramics, John Wiley, USA, 1976, p. 705.